Comprehensive Digital Twin of a Macro-fluidic Electrochemical Reactor to Optimize the Electrochemicalbased Recovery of O₂ from Metabolic CO₂

Jesus A. Dominguez
Insight Global/Jacobs Space Exploration Group (JSEG), Huntsville, AL, 35806

Shannon McCall Qualis Corporation /Jacobs Space Exploration Group (JSEG), Huntsville, AL, 35806

> Lorlyn Reidy, Mononita Nur, Brittany Brown NASA Marshall Space Flight Center, Huntsville, Alabama, 35811

Brian Dennis and Wilaiwan Chanmanee University of Texas at Arlington, ArlinFiguregton, Texas, 76019

Joseph Fillion, Kathryn Ollenburg Jacobs Space Exploration Group (JSEG), Huntsville, AL, 35806

Future long-duration missions will require a sustainable and efficient system capable of yielding a minimum of 75% O₂ recovery from metabolic CO₂ to achieve self-sufficiency for long space missions beyond Earth's low orbit1. A Macro-fluidic Electrochemical Reactor (MFECR) development effort to electrochemically recover O₂ from CO₂ is underway at NASA Marshall Space Flight Center (MSFC) to increase current O₂ recovery efficiency and reduce air revitalization (AR) system complexity at the International Space Station (ISS) habitat and future long missions. The authors have developed and deployed a digital twin of an actual single cell of the MFECR via a comprehensive 3D multiphysics model that thoroughly replicates the exact configuration and fluid/material domains of the MFECR. This model's electrochemical physics consists of multicomponent-multiphase electrochemical-driven reactions leading to CO₂ conversion to C₂H₄ and CO along with the formation of H₂ on the cathode in parallel with the generation of O2 and H2O on the anode. This electrochemical model is coupled with all the physics phenomena involved in the process, including but not limited to fluid and nonideal mass transfer of reactant and product species in free and porous media, convective/conduction/radiative heat transfer, and conduction of DC electrical current with Joule heating generation. The digital twin has proved to be an essential tool for performing different qualitative studies, including the effect of reducing the height (increasing the respect ratio) of the serpentine walls, leading to a further redesign of the EDU (the newly redesigned MFECR EDU has been fabricated and is expected to be used in future tests), the evaluation of setting different MFECRs connected in series, and the assessment of feeding air directly to the MFECR skipping the preceding metabolic CO₂ separation from air. The MFECR's test stand is fully automated and equipped with several inline measurements (flow, pressure, temperature, pH, component concentration) systems on all six MFECR's IO streams, allowing reliable experimental validation of the model, parametric determination of all electrochemical reactions, and process optimization.

Nomenclature

AR = atmospheric revitalization CDRS = carbon dioxide reduction system

CL = catalysis layer EC = electrochemical CO_2 = carbon dioxide C_2H_4 = ethylene

EDU = engineering design unit

ECLSS = environmental control and life support system

GC = gas chromatography GDL = gas diffusion layer GDE = gas diffusion electrode

CL = catalysis layer KOH = potassium hydroxide

MFECR = macro-fluidic electrochemical reactor

MPL = macropore layer

MSFC = Marshall Space Flight Center

NASA = National Aeronautics and Space Administration

OGA = oxygen generation assembly

 O_2 = oxygen OH = hydroxide ion

PDE = partial differential equations

Pt = Platinum

PTFE = poly-tetra-fluoro-ethylene

 H_2 = hydrogen

ISS = International Space station UTA = University of Texas at Arlington

I. Introduction

Removal of metabolic carbon dioxide (CO₂) is crucial in Atmospheric Revitalization (AR) at the ISS and any other livable space habitat to maintain a safe, breathable atmosphere inside the habitat. The critical objective for the AR system is to 'close the loop', that is, to capture gaseous human metabolic products, specifically water (H₂O) vapor and CO₂, for maximum O₂ recovery and to make other valuable resources from these products. The AR subsystem also removes trace chemical contaminants from the habitat atmosphere to preserve habitat atmospheric quality, provide O₂, and utilize instrumentation to monitor cabin atmospheric quality. Long-duration crewed space exploration missions will require critical advancements in AR process technologies to increase efficiency on O₂ recovery, reduce power and mass consumption, and increase reliability compared to prior AR processes for shorter missions typically limited to Low Earth Orbit (LEO). The AR in the International Space Station (ISS) includes four integrated units, which provide critical functions for life support, including Trace Contaminant Control (TCC) system, CO₂ carbon removal branded as Carbon Dioxide Removal Assembly (CDRA), O₂ generation branded as Oxygen Generation Assembly (OGA), and oxygen recovery branded as Carbon Dioxide Reduction System (CDRS).

The CDRS is a Sabatier reactor that operates at 300–400 °C and reduces CO_2 to methane (CH₄) and H₂O using H₂ from OGA (an electrolysis unit that generates O_2 as the main product and H₂ as a byproduct) as the reactant. The CDRS limits the feasibility of having a closed-loop system, as it requires more water than is metabolically generated, ultimately resulting in a recovery rate of approximately 50%. NASA Marshall Space Flight Center (MSFC) and the University of Texas at Arlington (UTA) are currently developing an Engineering Development Unit (EDU) of a Microfluidic Electro Chemical Reactor (MFECR) to convert a continuous stream of CO_2 and water into O_2 and C_2 H₄ at standard conditions. The novel design combines CO_2 conversion and water electrolysis (currently conducted in OGA and CDRS units, respectively) into one compact unit that runs at standard conditions and is theoretically capable of generating C_2 with a theoretical maximum metabolic CO_2 conversion of 73% while consuming less metabolic water. The metabolic CO_2 conversion process that currently operates at the ISS yields CC_2 as a waste byproduct, losing 4 moles of H (2 moles of H₂ originally generated by 2 moles of water) per 1 mole of C; the novel design yields C_2 H₄ as a byproduct losing half of the H/H₂ moles than the current CC_2 CH₄-byproduct-producer approach.

The authors have developed and deployed a digital twin that thoroughly replicates the actual configuration and fluid/material domains of the MFECR via a comprehensive 3D multiphysics model. In the model, the EC physics (multicomponent-multiphase electrochemical-driven reactions leading CO₂ conversion to C₂H₄ and CO and formation of H₂ on the cathode in parallel with formation of O₂ and H₂O on the anode) are coupled with all the other physics phenomena involved in the process including fluid and non-ideal mass transfer of reactant and product species in free and porous media, CO₂ transport from gas phase within porous electrode to liquid phase (electrolyte), condensation and evaporation of water driven by capillary pressure within porous medium, convective/conduction/radiative heat transfer, and conduction of DC electrical current with Joule heating generation.

This digital twin aims to perform comprehensive model-based studies to estimate the effect of proposed upgrades in the MFECR cell-stack configuration and process operation conditions on the O₂ recovery outcome. The authors

have upgraded the MFECR cell configuration based on the assessment, via this digital twin, of the effect of the respect ratio (width: height) of the serpentine path in all three MFECR cell chambers (cathode, anode, and electrolyte); the height of the serpentine path was decreased from 3.6 to 1.6 mm as the digital-twin-based assessment indicates that increasing the respect ration by reducing the path height to half leads to a substantial improvement in the O₂ recovery outcome. Other digital-twin-based evaluations conducted by the authors include the effect of a second cell connected in series with the primary one on the O₂ recovery outcome. Another digital twin assessment evaluated the feasibility of skipping the CDRA unit that removes the metabolic CO₂ from the air containing 1,500-3,000 ppm of CO₂ and feeds 100% of CO₂ to the MFCER.

II. Process Fundamentals

Catalysis developed by researchers at the University of Texas at Arlington (UTA) selectively reduces CO₂ to C₂H₄ via electrolysis at standard conditions using an alkaline electrolyte, potassium hydroxide (KOH), and yielding H₂

besides C₂H₄ on the cathode and O₂ on the anode¹. These three electrochemical (EC) reactions posted below indicate that hydroxide ions (OH⁻) are generated on the cathode via the reduction of CO₂ to C₂H₄ and H₂O to H₂, then transported through the electrolyte to the anode and consumed in the formation of O₂. While all OH⁻ generated on the cathode is consumed on the anode, H₂O consumed on the cathode is not entirely generated on the anode due to the formation of C₂H₄ byproduct yielding a net H₂O consumption (still lower than in the case of CH₄ byproduct generation in Sabatier's approach) as illustrated below.

GAS CHANNEL (CATHODE)

GAS DIFFUSION LAYER

CATALYSTLAYER

CATALYSTLAYER

CATALYSTLAYER

GAS DIFFUSION LAYER

OH

CATALYSTLAYER

GAS DIFFUSION LAYER

OAS DIFFUSION LAYER

OB

CATALYSTLAYER

OB

CATALYST

Figure 1. Schematic of EC process in the MFECR.

Figure 1 depicts a schematic of the EC process in the MFECR equipped with three flow streams that carry cathodic

CO₂ reactant, KOH electrolyte solution, and anodic O₂ product, respectively, along with two conducting gas diffusion electrodes (GDE) that have three layers, the gas diffusion layer (GDL), the macropore layer (MP), and the catalysis layer (CL) as illustrated in Figures 2a (GDE cathode) and 2b (GDE anode). The four experimental EC reactions observed in the cathode and the anode are included in the digital-twin model and listed below.

Cathode

$$2CO_2 + 8H_2O + 12e^- = C_2H_4 + 12OH^-$$
 (1)
 $CO_2 + H_2O + 2e^- = CO + 2OH^-$ (2)

$$2H_2O + 2e^- = H_2 + 2OH^-$$
 (3)

Anode

$$16OH^{-} = 4O_2 + 8H_2O + 16e^{-}$$
 (4)

$$\overline{3\text{CO}_2} + 3\text{H}_2\text{O} = \text{C}_2\text{H}_4 + \text{CO} + \text{H}_2 + 4\text{O}_2$$
 (5)

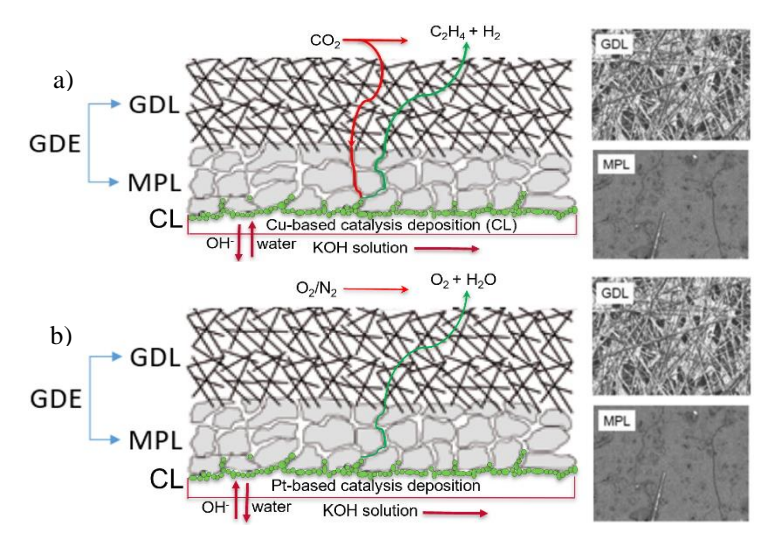


Figure 2. Schematic of GDL, MPL, and CL domains housing the species generated at the CL of the (a) GDE cathode and (b) GDE anode.

In the cathode channel, CO_2 diffuses through the GDL, reaching the MPL that houses the CL formed by EC deposition of copper-based catalysis in direct contact with the KOH aqueous-electrolyte flow stream to yield not only the reduction of CO_2 to C_2H_4 (reaction 1) and CO (reaction 2) but also the formation of H_2 (reaction 3) from H_2O . CO_2 , CO, and H_2 products diffuse back to the cathode channel, mixing with unreacted and depleted CO_2 gas stream.

In the anode channel, O_2 is generated (reaction 4) at the CL (coated with platinum/nickel and in direct contact with the aqueous-electrolyte flow stream). It diffuses throughout the GDL, reaching the anode gas flow stream. As indicated in the total reaction 5, the CO_2 reduction reactions (reactions 1 and 2) consume water to yield C_2H_4 , CO, H_2 , and O_2 , increasing OH^- concentration in the electrolyte stream and requiring water makeup to keep the desired OH^- concentration in the aqueous electrolyte. Researchers have reported other competing reactions on the cathode yielding different C_1 and C_2 products with copper-based catalysis²; UTA researchers have developed unique and proprietary copper-base d catalysis that selectively yields C_2H_4 over CH_4 contrary to other Cu-based catalysis reported in the literature³. CO and CH_4 are more undesired byproducts than C_2H_4 as the formation of CO reduces O_2 recovery, and the formation of CH_4 consumes more water than the formation of C_2H_4 since it has a lower H/C ratio, 2 for C_2H_4 and 4 for CH_4 . The model does not include the CH_4 reaction in the cathode as its compositions in the outlet stream using proprietary UTA's catalysis have shown to be lower than 0.005%.

III. Model Domains

The material domains used in the 3D model are replicas, at the Engineering Design Unit (EDU) scale, of the actual MFECR's material domains; the drawings generated to fabricate the MFECR's domain components were also used as spatial material domains in the 3D model, along with the commercial available GDE's domains bearing three subdomains (GDL, MPL, and CL) with spatial dimensions provided by their manufacturers.

The eleven MFECR's material domains include two non-electrical-conducting endplates to press the EDU on the cathode and anode ends respectively, two electrical-conducting serpentine channels to house the CO₂ (cathode) and O₂ (anode) gas flow streams, one non-electrical-conducting electrolyte serpentine channel to house the electrolyte liquid flow stream, and two GDEs (cathode and anode), each one housing three material subdomains that include the gas diffusion layer (GDL), the MPL, and the CL. MPLs are typically built up by a mixture of carbon black powder and a hydrophobic agent, poly-tetra-fluoro-ethylene (PTFE). GDL works as a protective layer for the delicate catalyst structure, provides good mechanical strength and easy gas access to the catalyst, and improves the electrical conductivity. MPL reduces the contact resistance between the catalyst layer and the microporous substrate.

Besides the eleven spatial material domains described above, the model includes three fluid domains flowing along the cathode, electrolyte, and anode serpentine chambers. These three flow domains were created by generating a solid

material domain of the entire MFECR and subtracting all eleven spatial material domains (two endplates, three serpentine channels, two GDLs, two MPLs, and two CLs). Each cathode and anode flow domain has three subdomains to house the cathode and anode streams throughout four different flow media, corresponding to one free flow along the serpentine channel and three porous flows along the GDL, MPL, and CL.

Figure 3 depicts the critical domains colored in purple: a) top and bottom endplates, b) cathode serpentine channel, c) cathode GDE (housing GDL, MPL, and CL subdomains), d) electrolyte serpentine channel, e) anode GDE (housing GDL, MPL, and CL

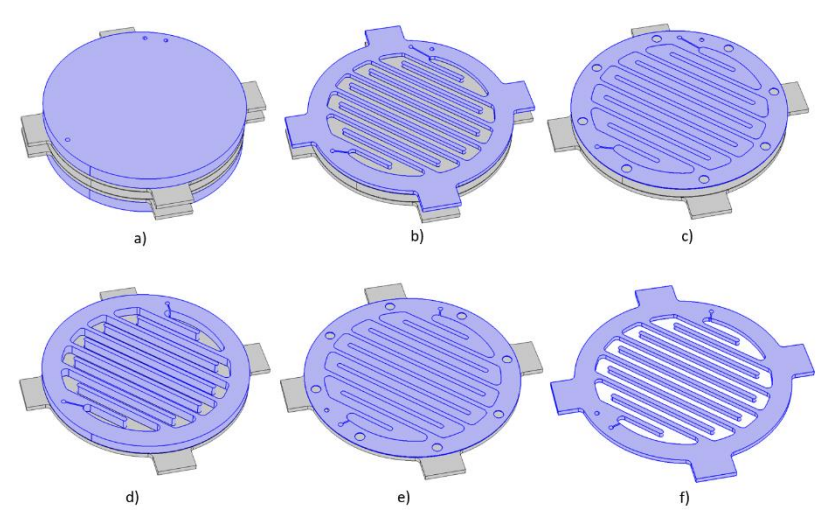


Figure 3. MFECR's model material domains (colored in purple): a) top and bottom endplates, b) cathode serpentine channel, c) cathode GDE (housing GDL, MPL, and CL subdomains), d) electrolyte serpentine channel, e) anode GDE (housing GDL, MPL, and CL subdomains), and f) anode serpentine

subdomains), and f) anode serpentine channel. The materials used in the actual MFECR elements and assigned to the corresponding model's material domains include polycarbonate for the endplates, Teflon for the electrolyte serpentine channel, nickel for the anode and cathode serpentine channels, and porous carbon-based composite for the GDEs. The physical properties of these material domains, including but not limited to density, thermal conductivity, heat capacity, electrical conductivity, and thermal radiative emissivity, are set in the model as temperature-dependent.

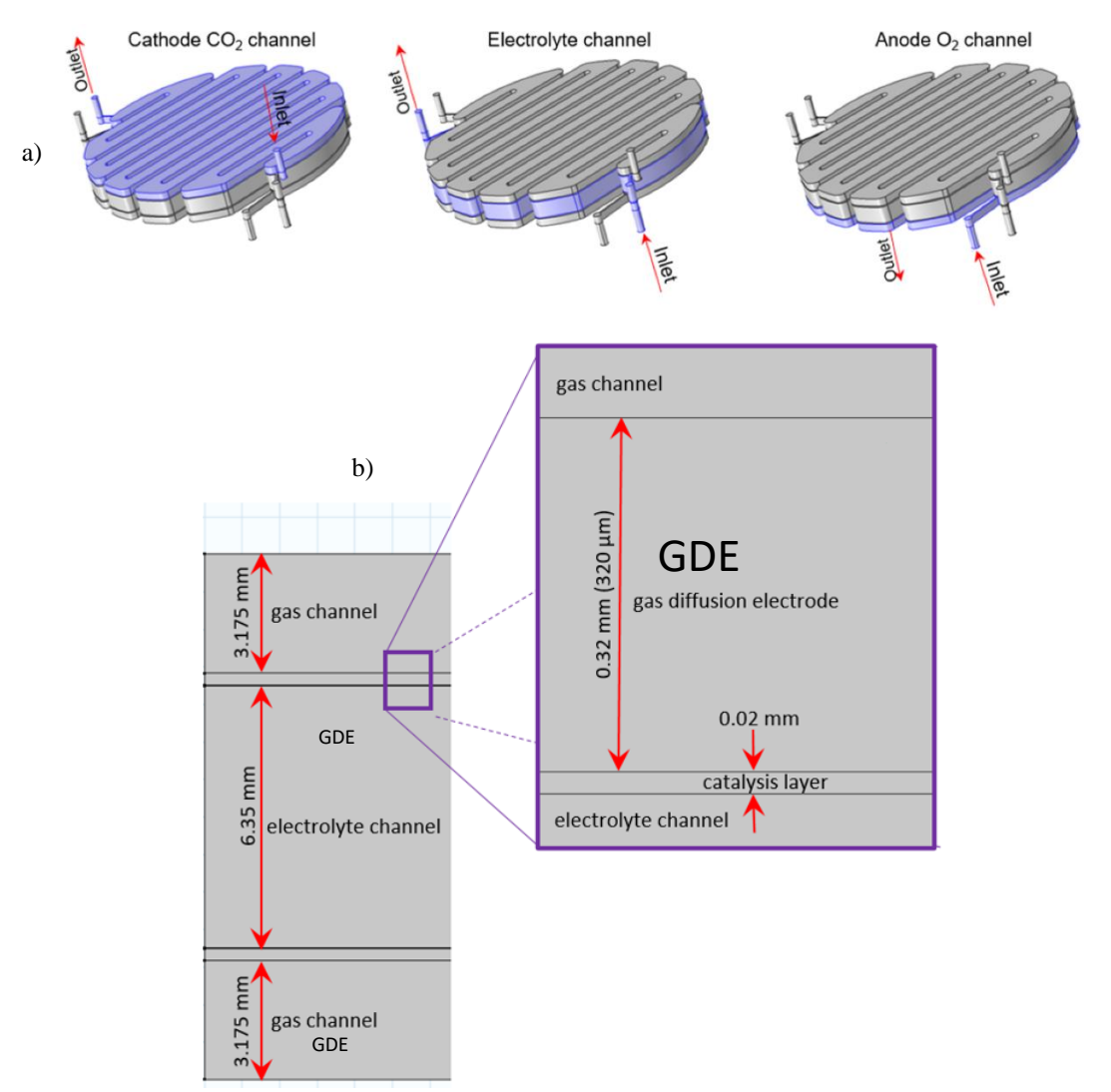


Figure 4. a) Flow domains and I/O streams for the cathode, electrolyte, and anode serpentine channels. b) Cross section of all domains, including the GDE domain, with their respective dimensions.

Figure 4a illustrates the flow domains and the direction of the IO flow streams in each serpentine channel corresponding to the cathode (CO_2 gas), electrolyte (aqueous KOH solution), and anode (O_2 gas); Figure 4b shows a cross-section of all model's domains, including the GDE domain, with their respective dimensions. As indicated in Figure 4b, the MFECR's digital-twin model has significant thickness scale differences between interconnected domains, from 6.35 mm of electrolyte to 0.02 mm of the CL. The physical properties of these domains, including but not limited to viscosity, thermal conductivity, electrical conductivity, diffusion coefficients, CO_2 solubility in electrolyte alkaline solution, and GDE's capillary pressure, are also temperature-dependent in the model.

Model Definition

The EC reaction section of the MFECR consists of two porous CLs and an electrolyte serpentine channel sandwiched in the middle, as shown in Figures 1 and 2. The CO₂ feeds the cathode serpentine channel, and part of the O₂ product is fed back to the anode serpentine chamber. The alkaline solution feeds the electrolyte serpentine chamber, wetting the CLs of both the anode and cathode GDEs and allowing the hydroxide ion (OH⁻) transport between them. The EC reactions in the cell are reactions (1), (2) and (3) in the cathode's GDE and reaction (4) in the anode's GDE, yielding the total reaction (5).

The model includes the following processes:

• Electronic charge balance (Ohm's law)

- Ionic charge balance (Ohm's law)
- Concentration-dependent Butler-Volmer and Tafel charge transfer kinetics
- Flow distribution in gas and liquid channels (Navier-Stokes)
- Flow in the porous GDL, MPL, and CL (Brinkman equations)
- Mass balances in the gas phase in both gas channels and porous GDL, MPL, and CL (Maxwell-Stefan diffusion and convection)
- Evaporation and condensation of water on the GDL and gas channels and condensed water transportation through the GDL's porous via capillary pressure.
- Temperature-dependent CO₂ absorption into KOH aqueous electrolyte via Henry constant.
- Temperature (energy balance equation) via three types of heat transfer mechanisms,
 - 1) conductive within EDU's components,
 - 2) convective within the channel flows,
 - 3) radiative between EDU surface and ambient
- Heat generation/source via Joule heating effect.

A. EC Reaction Phase

Species generated in the cathode are gaseous, C_2H_4 , CO, and H_2 via reactions 1, 2, and 3, respectively; in the anode, two species are generated via reaction 4, gaseous H_2 and water vapor. The model estimates the temperature-pressure-dependent condensation of the water vapor generated at the anode (reaction 4) and its transportation through the porous GDE and MPL domains driven by the porous capillary pressure. In the CO_2 reduction (CO_2R) to C_2H_4 (reaction 1) the CO_2 reactant is still assumed to be in the gas phase but dissolved in the aqueous KOH electrolyte as recent experimental and theoretical work has demonstrated the importance of water and hydrated cations on the elementary processes involved in CO_2R superseding the role of CO_2 gas phase within the GDLs. Therefore, researchers have proposed that the catalyst must be covered with electrolytes to be active; this means that although CO_2 is supplied to the GDE from the gas phase, the reactant at the catalyst site is still dissolved in CO_2 .

B. Charge Balances

The electronic and ionic charge balance in the cathode and anode current feeders, the electrolyte, and GDEs are solved using a secondary current distribution interface that accounts for the effect of the electrode kinetics and solution resistance. The model assumes that concentration-dependent Butler-Volmer charge transfer kinetics describes the charge transfer current density for the EC reactions except for CO₂, as the EC reaction is believed to take place in the gas phase but diluted in the KOH electrolyte solution wetting the catalysis electrochemically deposited on the GDE's MPL. At the cathode, CO₂ is reduced to C₂H₄, CO, and H₂ is concurrently formed as stated in Butler–Volmer reactions (1), (2), and (3), respectively, assuming that the concentrations at the electrode are practically equal to the concentrations in the bulk electrolyte, allowing the current to be expressed as a function of potential only:

$$i_{c,c_{2}h_{4}} = i_{o,c_{2}h_{4}} \left(\frac{c_{co_{2}}}{c_{co_{2},ref}} exp\left(\frac{\alpha_{c,co_{2}}F}{RT} \eta \right) - \frac{c_{c_{2}h_{4}}}{c_{c_{2}h_{4},ref}} exp\left(\frac{-\alpha_{a,co_{2}}F}{RT} \eta \right) \right)$$
(6)

$$i_{c,co} = i_{o,co} \left(\frac{c_{co_2}}{c_{co_2,ref}} exp\left(\frac{\alpha_{c,co_2}F}{RT} \eta \right) - \frac{c_{co}}{c_{co,ref}} exp\left(\frac{-\alpha_{a,co_2}F}{RT} \eta \right) \right)$$
 (7)

$$i_{c,h_2} = i_{o,h_2} \left(\frac{c_{h_2}}{c_{h_2,ref}} exp\left(\frac{\alpha_{c,h_2}F}{RT} \eta \right) - exp\left(\frac{-\alpha_{a,h_2}F}{RT} \eta \right) \right)$$
(8)

Here i_{o,co_2} $i_{o,co}$ and i_{o,h_2} are the cathode standard exchange current densities (A/m²) for the cathode reactions (1), (2), and (3), c_{co_2} c_{co} , $c_{c_2h_4}$ c_{h_2} are the molar concentrations of CO₂, C₂H₄, and H₂ respectively, $c_{co_2,ref}$ and $c_{c_2h_4,ref}$ are the reference concentrations (mol/m³). α_{c,co_2} α_{a,co_2} α_{c,h_2} α_{a,h_2} are the cathodic/anodic charge transfer coefficients for the cathode reactions (1), (2), and (3) respectively. Furthermore, F is Faraday's constant (C/mol), R the gas constant (J/(mol·K)), T the temperature (K), and η the overpotential (V).

For the anode, the following charge transfer kinetics equation applies for reaction (4)

$$i_{c,o_2} = i_{o,o_2} \left(\frac{c_{o_2}}{c_{o_2,ref}} exp\left(\frac{\alpha_{c,o_2}F}{RT} \eta \right) - exp\left(\frac{-\alpha_{a,o_2}F}{RT} \eta \right) \right)$$
(9)

Here i_{o,o_2} is the anode exchange current density (A/m^2) for the anode reaction (3), c_{o_2} is the molar concentration of O_2 , $c_{o_2,ref}$ is the reference concentration (mol/m³). α_{c,o_2} α_{a,o_2} are the cathodic/anodic charge transfer coefficients. The overpotential η is defined as

$$\eta = \Delta \phi_{electronic} - (\Delta \phi_{ionic} + \Delta \phi_{eq}) \tag{10}$$

Where $\Delta \phi_{eq}$ is the equilibrium potential difference (SI unit: V). The concentration-dependent kinetics expressions (6), (7), (8), and (9) are used to set up the charge transfer expressions that lead to $\Delta \phi_{ionic}$ value.

At the cathode's inlet boundary, the potential is set at a reference potential of zero (ground). At the anode's inlet boundary, the potential is set to the cell potential V_{cell} . The cell polarization V_{pol} is then given by

$$V_{pol} = (\Delta \phi_{eq,c} - \Delta \phi_{eq,a}) - V_{cell} \tag{11}$$

Where $\Delta \phi_{eq,c}$ and $\Delta \phi_{eq,a}$ are the total equilibrium differential potential of all individual species participating in the EC reactions on the cathode and the anode, respectively.

C. Multicomponent Transport

At the cathode serpentine channel, CO_2 gas is supplied as a reactant, meaning that the gas in the channel and GDE consists of three components: unreacted CO_2 and products C_2H_4 and H_2 . In the anode, the O_2 product is resupplied and composed of two product components: O_2 and water vapor. Nitrogen (N_2) is a carrier gas for O_2 and water vapor products.

Maxwell-Stefan's diffusion and convection equations describe the material transport, solved using a transport of concentrated species interface for each electrode flow serpentine channel. The boundary conditions at the walls of the gas channel and GDE are zero mass flux (insulating condition). The composition is specified at the inlet, while the outlet condition is convective flux. This assumption means the convective term dominates the transport perpendicular to this boundary. Continuity in composition and flux applies to all mass balances at the interfaces between the GDEs and the serpentine channels.

D. Gas and Liquid Flow Equations

The Brinkman equation describes flow in porous media where momentum transport by shear stresses in the fluid is essential. The model extends Darcy's law to include a term that accounts for the viscous transport in the momentum balance and introduces velocities in the spatial directions as dependent variables. The Brinkman equations interface is used in the model to solve the velocity field and pressure in both the cathode and anode serpentine channels.

The compressible Navier-Stokes equations govern the flow in the open channel sections and the Brinkman equations in the porous GDEs. Couplings for the density, velocity, pressure, and net mass sources and sinks are made for the transport of concentrated species interfaces by using reacting flow multiphysics. The incompressible Navier-Stokes equations govern the liquid flow in the electrolyte serpentine channel.

E. Heat Transfer Equations

A general energy balance equation is implemented in the model to obtain the temperature distribution throughout the MFECR, including all solid parts and three flows running through the cathode, anode, and electrolyte serpentine channels. The model considers two heat transfer mechanisms for the heat exchange between the MFECR's surface and the ambient, natural convection and thermal radiation. For natural convection, constant heat transfer coefficients are initially assumed based on values found in the literature and finally determined via experimental validation using modeled and experimentally measured temperature values throughout the MFECR's surface. Thermal radiation emissivity of the MFECR's materials is not found in the literature. It is used in the model to compute the radiative heat transfer mechanism between MFECR's surface and the ambient.

As an electrical potential is applied between the two GDEs, an electrical current is generated and carried throughout the walls of the cathode, anode, and electrolyte serpentine channels. The model accounts for this energy source transformed in heat generation via the Joule heating effect equation.

IV. Model Implementation

The 3D model was implemented in COMSOL⁴, a cross-platform finite element analysis, solver, and multiphysics simulation software. It allows conventional physics-based user interfaces and coupled systems of partial differential equations (PDEs). COMSOL provides an integrated development environment (IDE) and unified workflow for electrical, mechanical, fluid, acoustics, and chemical applications.

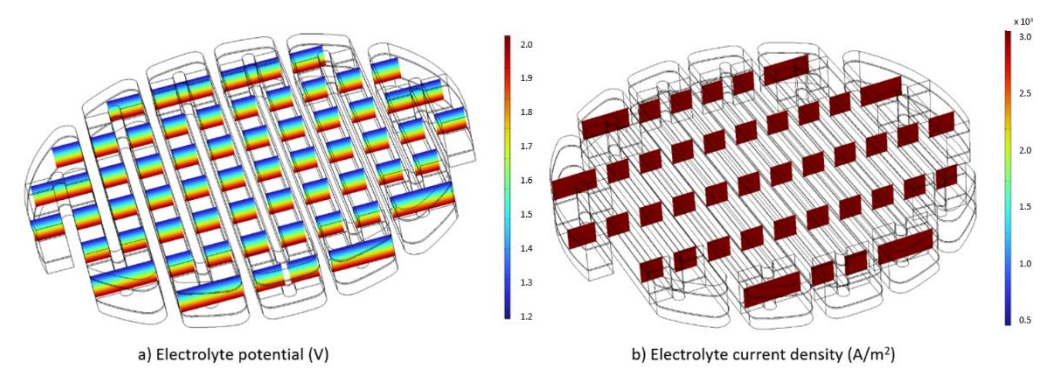


Figure 5. Potential and current density on electrolyte solution as 4 Volts are applied to the MFECR.

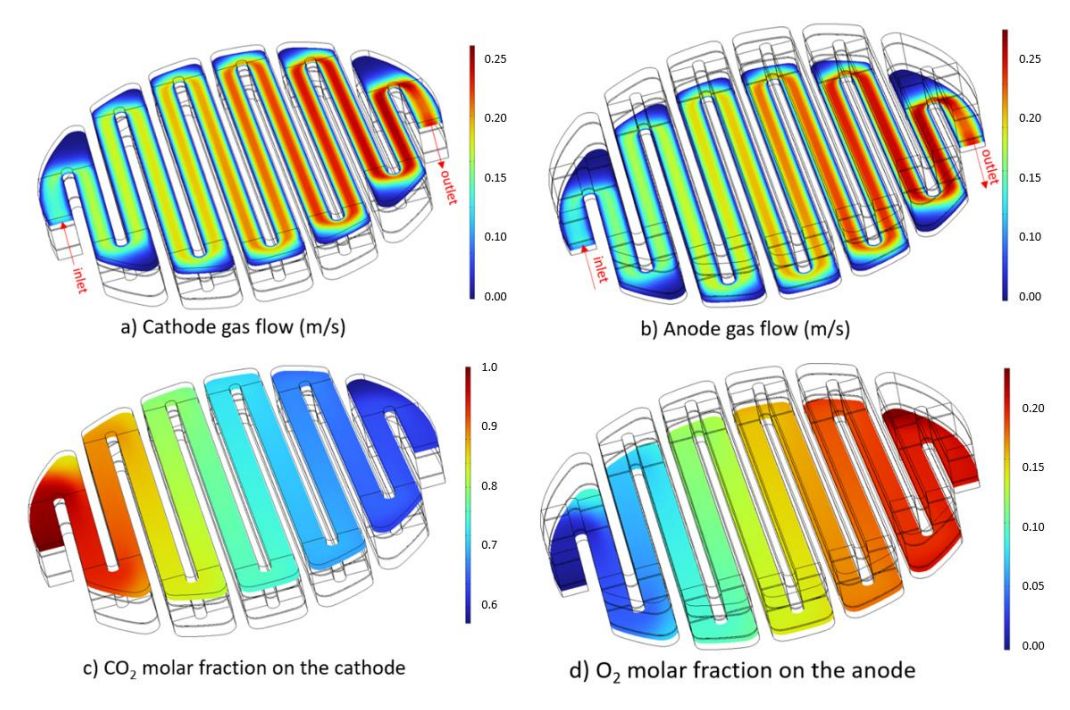


Figure 6. Gas flow profiles through the cathode (a) and the anode (b) serpentine channels as 100 sccm of CO_2 and N_2 are fed to the cathode and anode gas channels respectively; CO_2 (c) and O_2 (d) weight fraction profiles through the cathode and the anode gas channels a) and b) respectively.

Figure 5 illustrates the electrolyte potential (5a) and current density (5b) as an electrical potential of 4 Volts is applied on material domains 2b and 2f corresponding to the cathode and the anode serpentine channels, respectively. Figures 6a and 6b depict the gas flow profiles (m/s) through the cathode and the anode flow domains illustrated in Figure 4 as

100 sccm of CO₂ and 100 sccm of N₂ are fed to the cathode and anode gas channels, respectively; Figures 6c and 6d depict the CO₂ and O₂ weight fractions within the cathode and the anode gas channels respectively.

The Brinkman equation is used to solve the velocity field and pressure in both the cathode and anode serpentine channels, as these gas flows, have two regimes: free flow in the hollow channel and porous flow in the GDE. The Navier-Stoke equation with laminar flow assumption is used to solve the aqueous solution's velocity field and pressure in the electrolyte serpentine channel.

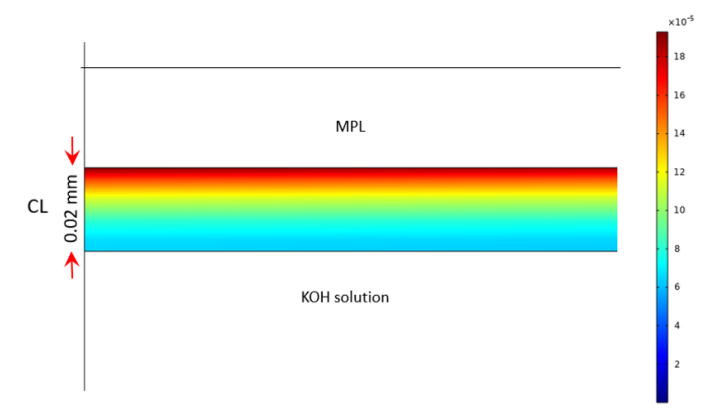


Figure 7. Absorbed CO_2 (M) within the KOH solution wetting the cathodes's CL

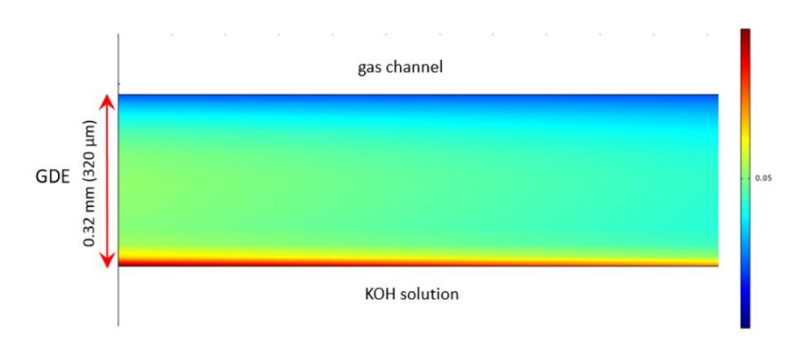


Figure 8. Volumetric condensed water (-) within the anode GDE

As illustrated in Figure 6, CO_2 depletes at the expense of the C_2H_4 and CO generation along with H_2 byproduct from water electrolysis, enriching the cathode gas flow with C_2H_4 , CO, and H_2 as the CO_2 and H_2O continue reacting, yielding C_2H_4 , CO and H_2 , respectively and flowing toward the channel's end. As stated above, temperature-dependent CO_2 absorption into KOH aqueous electrolyte via the Henry constant is included in the model to determine the absorbed CO_2 that is the actual reactant in reactions 1 and 2. Figure 7 shows the cross-section profile of the CO_2 absorbed CO_2 that is the Actual reactant in reactions 1 and 2. Figure 7 shows the cross-section profile of the CO_2 absorbed CO_2 with a thickness of CO_2 mm CO_2

 C_2H_4 , CO_1 and H_2 , once generated on the CL coated with copper-based catalysis, diffuse through the MPL and GDL to reach the serpentine channel and mix with the flowing CO_2 -depleted gas stream, as illustrated in Figure 2. On the anode serpentine-channel side, O_2 is generated on the CL coated with Platinum/Nickel (Pt/Ni) and diffused through the MPL and GDL, reaching the carrier (N_2) gas used to feed the anode serpentine channel.

Water vapor is generated in the anode GDE via reaction 4, and a fraction of this water vapor is turned into the liquid phase as it reaches saturation induced by the pressure along the capillary formed in the GDE; many capillary pressure correlations have been suggested for various $GDLs^6$. The model uses the approach determined by Nguyen⁷. Figure 8 shows the volumetric liquid of saturated water (-) within a cross-section of an anode GDE with a thickness of 0.32 mm (320 μ m).

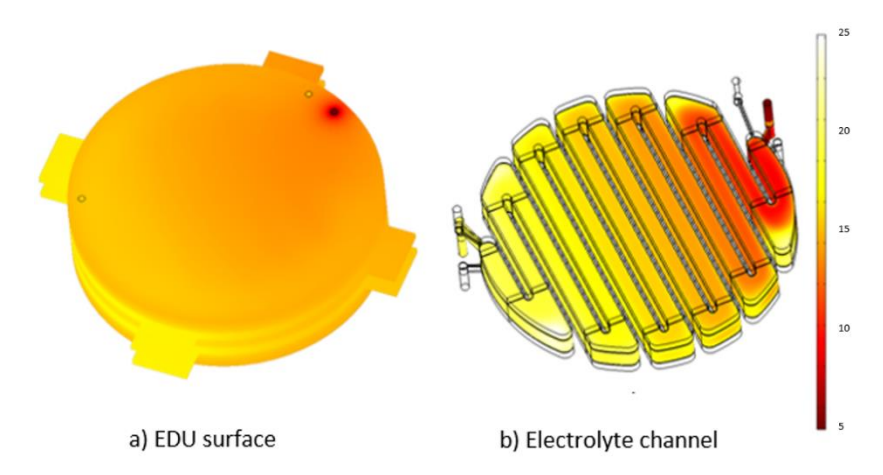


Figure 9. Temperature (degrees Celcius) profile throughout the a) MFECR's surface and b) electrolyte serpentine channel as KOH solution is fed to the electrolyte serpentine channel at 5 degrees Celcius having an ambient temperature of 27 degrees Celcius.

Figure 9 depicts the temperature profile of the a) MFECR's surface and b) electrolyte KOH solution flow that is fed at 5 degrees Celcius, having set at an ambient temperature of 27 degrees Celcius. The model considers two sources of heat exchange with the environment (natural convection and thermal radiation) and one heat source (Joule heating effect). The model uses different constant natural convective heat transfer coefficients on three MFECR's surface areas, two (horizontal and vertical) open areas, and one horizontal area underneath. The value of each of these three coefficients will be experimentally determined through experimental validation by measuring temperature throughout the MFECR's surface. As illustrated in Figure 9a, the cold electrolyte feed stream generates a cold spot on the MFECR's endplate surface. Figure 9b shows that the electrolyte temperature increases as the KOH solution flows toward the electrolyte channel's exit due mainly to heat flux gained from the ambient (natural convection and thermal radiation) and the Joule-heating effect.

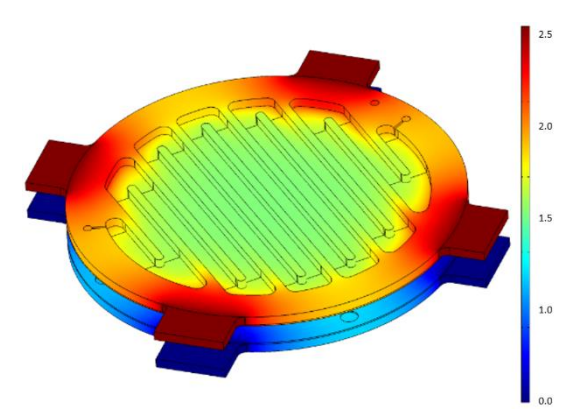


Figure 10. Electrical potential on serpentine channels and GDEs as a potential difference of 2.5 V is applied to the channel's ears.

As electrical potential is indeed applied on each of the four ears of both (cathode and anode) serpentine channel domains shown in Figures 3b and 3f, respectively, the actual differential potential within the EC cell (between the two GDEs) happens to be lower than the electrical potential applied on the ears as the two joint materials (nickel-based channel and carbon-based GDE) have different density and electrical conductivities. The model correctly sets the experimental operating potential value as boundary conditions on the ear's surface. As illustrated in Figure 10, a potential of 2.5 V is applied to each of the four ears of the cathode serpentine channel (dark red region) while ground (0 V) is applied to the anode (dark blue). The modeled electrical potential decreases substantially on the GDE surface, that is, the floor of the serpentine channel, from 2.5 V to 1.6 V (light yellow region) near the body-channel wall and 1.4 V (light green) along the serpentine channel.

V. Model Validation

The model developed and deployed by the authors at MSFC has the multiphysics foundations and rigor to simulate the actual EC process, allowing the user to optimize the design and operation of the MFECR aimed and manufactured at the EDU scale to efficiently yield metabolic CO_2 reduction to C_2H_4 and CO and generate H_2 and O_2 as byproducts at ambient conditions. The MFECR is installed in a test stand at MSFC equipped with all the instrumentation and sensors that will allow the validation of the model, including determining the EC kinetics parameters for the critical EC reactions that occur on the cathode and the anode CL domains.

All inlet-outlet (IO) streams of the MFECR are fully monitored inline yielding and logging data on a) flow rate, temperature, and pressure for all IO streams, b) pH on both input and output KOH solution streams, and c) gas composition on the cathode and anode outlet gas streams. The IO streams include 1) the inlet CO_2 gas and outlet product streams at the cathode serpentine channel, 2) the inlet O_2 carrier gas and the outlet product streams at the anode serpentine channel, and 3) the inlet and outlet KOH-solution streams at the electrolyte serpentine channel.

Assuming electron transfer is the rate-determining step on both GDEs, the concentration-dependent Butler-Volmer charge-transfer kinetics yields three parameters (exchange current density i_o, cathodic charge transfer α _c, and anodic charge transfer α _a) for each one of the three EC reactions considered in the MFECR's model, reactions 1 (CO₂ reduction), 2 (H₂ formation) and 3 (O₂ formation).

VI. Digital-Twin-based Assessments

A. MFECR Respect Ratio

The MFECR's digital twin assessed an increment in the MFECR respect ratio (width: height) of the serpentine path of all three chambers (cathode, anode, and electrolyte). Two path wall heights were assessed, the current one, 3.2 mm, and a half-reduced one, 1.6 mm, keeping the same width, 4 mm, increasing the MFECR's path respect ratio from 1.25 to 2.5 and using the same inlet pure CO_2 inlet flow rate in both path respect ratios and width (4 mm) as well as length (900 mm) of the serpentine path. Figure 11 summarizes the outlet composition in both assessment cases, 3.2 and 1.6 mm path height, respectively; the C_2H_4 outlet composition substantially increases as the respect ratio rises from 1.5 (3.6 mm height) to 2.5 (1.6 mm height).

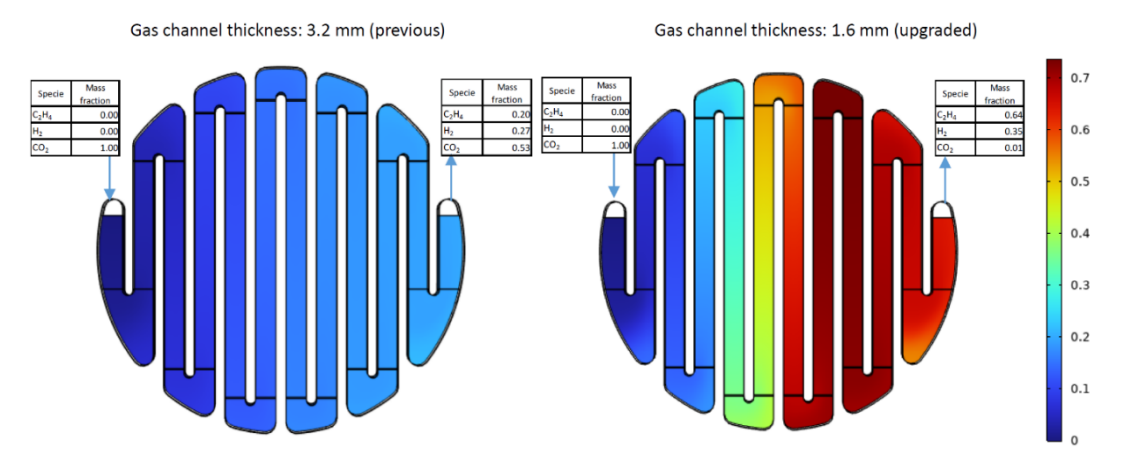


Figure 11. Outlet composition in both assessment cases, 3.2 and 1.6 mm path height, respectively.

As the above digital-twin-based assessment indicates (Figure 11), reducing the serpentine-path height of the serpentine path of the MFECR used in these preliminary tests from 3.2 to 1.6 mm leads to the increment of the C_2H_4 generation (and the O_2 recovery). The MFECR has been upgraded and fabricated with a serpentine path height of 1.6 mm and is expected to be used in future tests.

B. Addition of MFECR cells connected in series

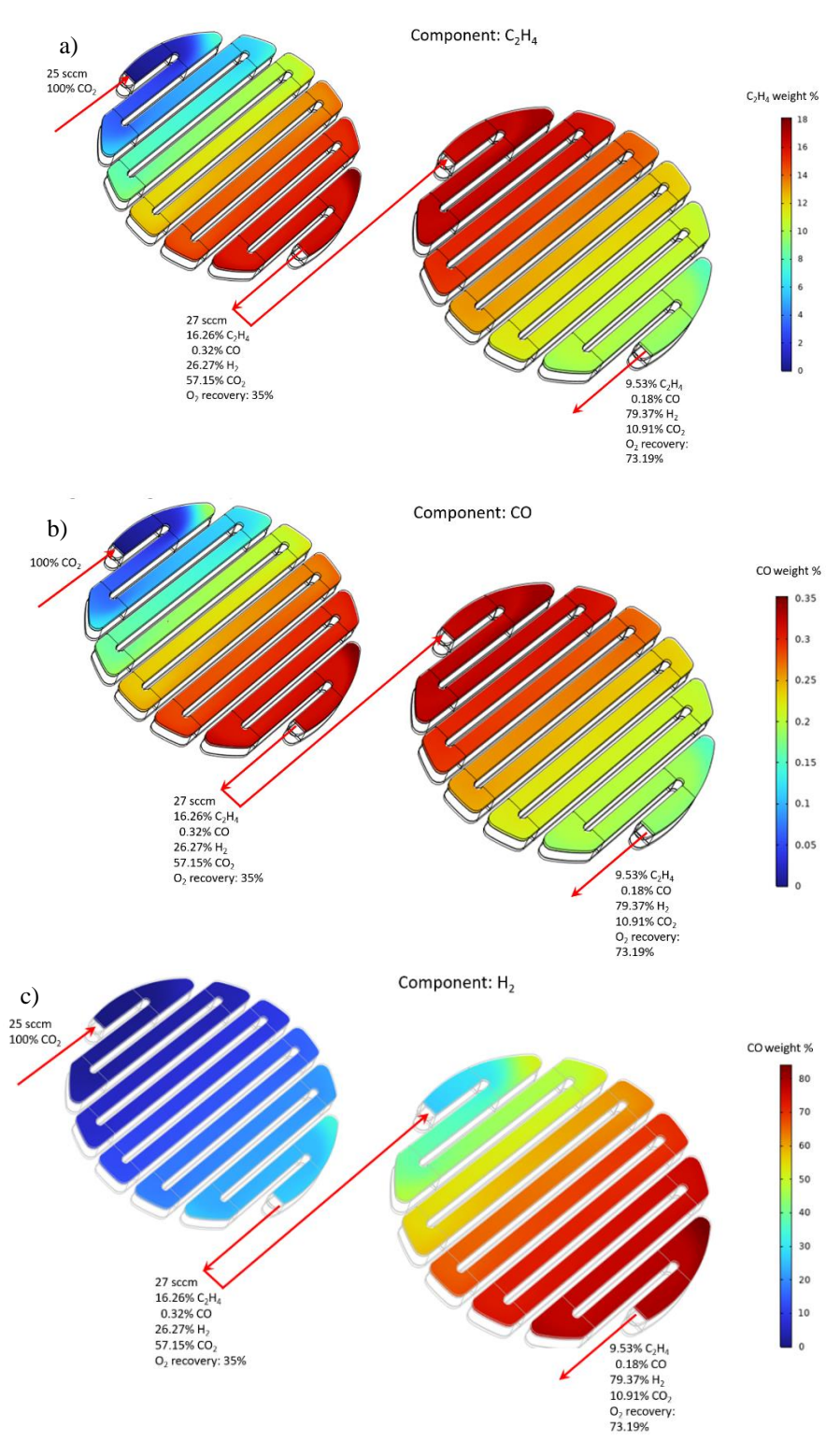


Figure 12. Digital-twin-based O_2 recovery outcome by generating a) C_2H_4 , b) CO, and c) H_2 in the cathode, leading to an O_2 recovery of 35% in the first cell and an increase to 73.19% in the second cell.

An alternative to increase the recovery of O₂ is to add MFERC's cells connected in series, in which the outlet stream of the preceded cell becomes the inlet stream of the subsequent cell. The digital twin was used to assess the outcome of the O₂ recovery and the side effects of this alternative. Figure 12 summarizes the O₂ recovery outcome by generating C₂H₄, CO, and H₂ in the cathode, leading to an O₂ recovery of 35% in the first cell and an increase to 73.19% in the second cell. As CO₂ is substantially depleted in the second cell, the water electrolysis becomes the predominant one, making H₂ the most extensive outlet composition in the cathode of the second cell. One side effect of using two cells connected in series is the excess H₂ generation in the second cell, besides the fact that the mass and volume of the MFECR stack increase.

C. Direct air inlet to MFECR stack

The digital twin of the MFECR single cell built/deployed via a comprehensive 3D model was used to theoretically assess the O₂ recovery from CO₂ using 3,000-6,500 ppm of metabolic CO₂ in air (concentration aboard the ISS) instead of 100% (concentration currently obtained from the CDRA after the removal of 3,000-6,500 ppm of metabolic CO₂ from the air). The theoretical evaluation shows that a stack of MFECRs can handle direct air feed with 3,000– 6,500 ppm of metabolic CO₂ and obtain equivalent O₂ recovery than a smaller stack of MFECRs handling 100% CO₂ from the CDRA. An additional study was performed using not the CO₂ concentration in the ISS (3,000–6,500 ppm) but the CO₂ level in atmospheric air (400 ppm). Figure 13 summarizes the estimated outcome of a single MFECR cell as atmospheric air containing 400 ppm of CO₂ is fed to a single MFECR cell; two sets of parameters for the Butler-Volmer exchange current density equations (1) through (4) were used in the study, one set assumes standard exchange current densities of 1E-5 and 1E-11 A/m² for C₂H₄ and CO respectively, the second set assumes a more favorable conversion of CO₂ to C₂H₄ and CO with standard exchange current densities of 1E-3 and 1E-10 A/m² for C₂H₄ and CO respectively. For a lower standard exchange current densities of 1E-5 and 1E-11 A/m² for C₂H₄ and CO, respectively, in both cases (400 ppm and 100% inlet CO₂) will be required, a second cell connected to this cell to increase CO2 reduction. For higher (more favorable) standard exchange current densities of 1E-3 and 1E-10 A/m² for C₂H₄ and CO, respectively, in the case of 400 ppm CO₂ inlet, a single cell would be capable of reducing the entire CO_2 inlet (400 ppm).

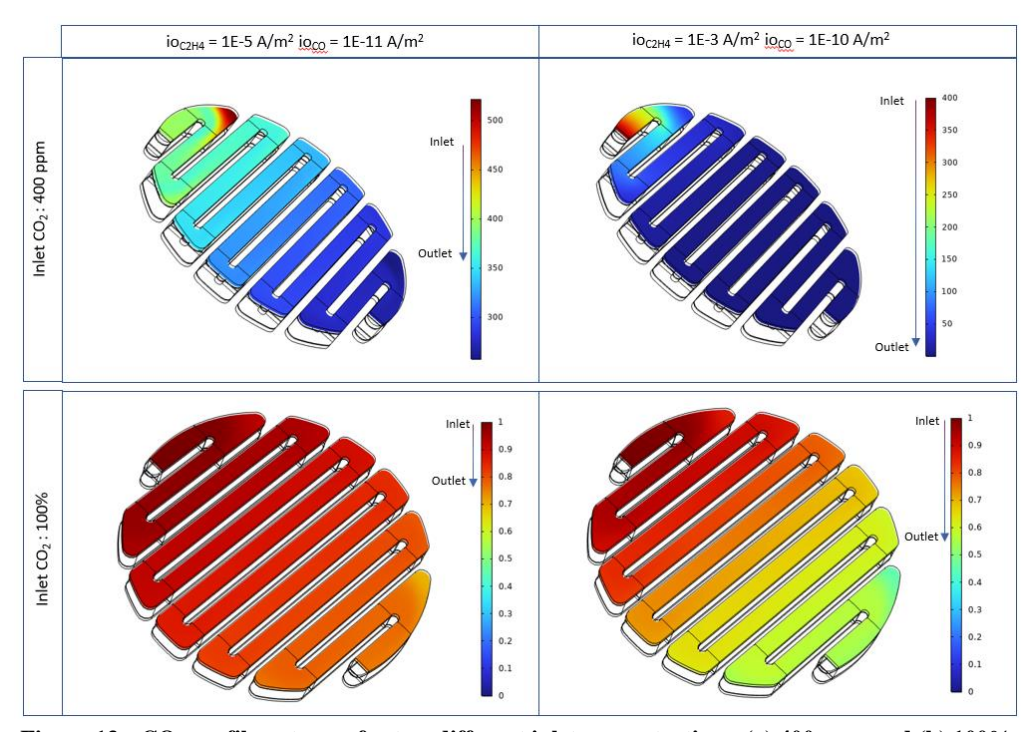


Figure 13. CO₂ profile outcome for two different inlet concentrations, (a) 400 ppm and (b) 100% and two different sets of parameters for the Butler-Volmer exchange current density equations 1) and 2).

Summary and Conclusions

The ECLSS team has developed and deployed a digital twin that replicates the actual MFECR via a comprehensive and rigorous 3D multiphysics model for EC CO_2 conversion to C_2H_4 and CO and the formation of H_2 on the cathode along with the formation of O_2 and H_2O on the anode. The MFERC's digital twin has the foundation and rigor to simulate the EC process and optimize the design and operation of the EDU, allowing efficient metabolic CO_2 reduction to C_2H_4 , generating H_2 , CO, and O_2 as byproducts at ambient conditions.

The digital twin has proved to be an essential tool for performing different qualitative studies, including the effect of reducing the height of the serpentine walls, leading to a further redesign of the EDU (the newly redesigned MFECR EDU has been fabricated and is expected to be used in future tests), the evaluation of setting different MFECRs connected in series, and the assessment of feeding air directly to the MFECR skipping the metabolic CO_2 separation from air.

The validation of the model will determine the degree of uncertainty on the model; the experimental data matrix intended to be used to validate the model has enough data points within the range of the anticipated process conditions that the model uncertainty is expected to be adequate to use in process optimization.

Acknowledgment

We thank Dr. Enrique Jackson for his valuable participation and contribution to the modeling effort via high-performance computational machine.

References

- ¹ Brown B. R., Curreri P. A., Rabenberg E. M., Dominguez J. A., Reidy L. P., Dennis B., Chanmanee W., Burke K. A., Developmental efforts of an electrochemical oxygen recovery system for advanced life support, International Conference on Environmental Systems (ICES), 2021, 50th International Conference on Environmental Systems, paper 74, pp. 11-12.
- Y. Hori: Electrochemical CO₂ reduction on metal electrodes. In Modern Aspects of Electrochemistry, Vol. 42, C.G. Vayenas, R.E. White, and M.E. Gamboa-Aldeco, eds. (Springer, New York, 2008); pp. 89-189.
- ³ Tacconia N. R., Chanmanee W., Dennis B., Rajeshwarb K., Composite copper oxide–copper bromide films for the selective electro-reduction of carbon dioxide, J. Mater. Res., Vol. 32, No. 9, May 15, 2017; pp. 1727-1724
- COMSOL, Electrochemistry Module User's Guide, Software Manual User Guide, Version: COMSOL 5.4, 2018. https://doc.comsol.com/5.4/doc/com.comsol.help.echem/ElectrochemistryModuleUsersGuide.pdf
- Subramanian S., Li M., Yang K., Sassenburg M., Geometric Catalyst Utilization in Zero-Gap CO₂ Electrolyzers, ACS Energy Lett. 2023, 8, 222–229.
- ⁶ C. Si, X.-D. Wang, W.-M. Yan, and T.-H. Wang, Journal of Chemistry 2015, 1 (2015).
- ⁷ T. V. Nguyen, G. Lin, H. Ohn, and X. Wang, Electrochemical and Solid-State Letters 11, B127 (2008).